SHALE GAS STORAGE IN NANO-ORGANIC PORES WITH SURFACE

HETEROGENEITIES

A Thesis

by

DAHIYANA CRISTANCHO ALBARRACIN

Submitted to the Office of Graduate and Professional Studies of
Texas A&M University
in partial fulfillment of the requirements for the degree of

MASTER OF SCIENCE

Chair of Committee,	I. Yucel Akkutlu
Committee Members,	Maria A. Barrufet
	Yalchin Efendiev
Head of Department,	A. Daniel Hill

May 2017

Major Subject: Petroleum Engineering

ABSTRACT

Recent advances in drilling and well stimulation technologies have led to rapid development of shale formations as an important natural gas resource. However a comprehensive understanding of the source rock geochemistry is currently needed in order to identify key factors in resource shale hydrocarbon assessment and production forecasting. Previous works indicated that significant amount of methane is stored in kerogen in adsorbed state. Adsorption is controlled by surface area and surface properties of the kerogen nanopore walls. In this paper using molecular simulations we investigate the influence of surface chemistry and heterogeneity on methane storage in model kerogen pores. The results show excess amount of methane due to nanopore confinement effect is found to be most pronounced under the subsurface conditions when the reservoir pore pressure is in the range of 1,000-5,000 psi. Among the investigated surface heterogeneities, nitrogen-doped graphene surfaces are the most influential on methane storage. Doping affects strongly the Langmuir parameters related to the adsorption capacity. These results indicate that kerogen maturation and the associated changes in its composition have the potential to impact gas storage in resource shale formations. The work gives new insights into the potential impact of the surface chemistry on natural gas storage in kerogen and emphasizes the significance of source rock geochemistry.

DEDICATION

To all the Women in Oil and Gas Industry

ACKNOWLEDGEMENTS

NOMENCLATURE

CH$_2$Cl$_2$	Dichloromethane
CH$_3$OH	Methanol
V_{LJ}	The Lenard Jones potential energy
r	The distance between methane and the wall
ε	The minimum energy at an equilibrium distance
σ	The distance at which the potential energy is zero
MP2	Møller-Plesset correlation energy correction
6-31(g)	Six three one gi basis-set
GCMC	Grand Canonical Monte Carlo
TraPPE-UA	Trappe United Atom Force Field
N_A	The Avogadro number
M_{CH4}	The molecular weight of methane
ρ_{number}	The number density of methane
n_{excess}	The excess mass of methane molecules
$\rho_{bulk-CH4}$	The bulk density mass of methane from NIST
NIST	National Institute of Standards and Technology
$\rho_{calc-CH4}$	The calculated mass density of methane
$V_{3.8}$	The volume segment of methane molecule within the slit-pore.
G_a	The adsorbed-gas amount in moles
G_{sL}	The Langmuir storage capacity in moles

p	The pore pressure
p_L	The Langmuir pressure that is given in psi.
$(\rho_{calc-CH4})$	The methane mass density within the slit-pore
STM	Scanning Tunneling Microscopy
BHP	Bottom Hole Pressure

TABLE OF CONTENTS

LIST OF FIGURES

LIST OF TABLES

1. INTRODUCTION

1.1 Shale

Shale is a fine-grained sedimentary rock that is formed by the accumulation of sediments at the Earth's surface; with low matrix permeability in the order of nano-darcy (Alexander et al. 2011). It has recently become a strategically important natural gas resource in North America. Shales are source rocks and they have been responsible for in-situ generation of the natural gas which has been the product of thermally -and biologically- driven chemical reactions that have taken place in the organic constituents of shale, also known as kerogen Natural gas consists primarily of methane and other hydrocarbons like ethane and propane and non-hydrocarbon gases like carbon dioxide and nitrogen. Shale has large amount of organic material than other rocks and due to its low permeability, this rock forms a cap for hydrocarbon traps. The quality of shale reservoirs depend on several factors such as: thickness, organic content, thermal maturity, depth, pressure, fluid saturations, and permeability.

_____

1.2 Kerogen

Kerogen is an insoluble and porous organic material from which petroleum and natural gas are generated. It is by far the largest amount of organic material on earth (Durand 1980) and has recently become an important research topic related to studies in predicting how much oil and gas are stored underground. Kerogen does not have a well-defined specific chemical formula instead it is a mix of organic materials with some inorganic naturally-occurring atoms such as N, O, S. Having said that kerogen composition is sensitive to the level and stages of maturation. Chemical changes occur in the structure of kerogen with maturation which include loss of oxygen, nitrogen and sulfur, which leads to change in the functional groups in the structure of kerogen.

Petroleum fractions such as heavy oil and bitumen, are soluble in common organic solvents while kerogen is not. Hence, the separation of petroleum from kerogen has been done using solvent extraction methods. The extraction depends on the polarity of the solvent used and also on the analytical procedure that is applied. CH_2Cl_2 mixed with CH_3OH are solvents that are often used for the extraction of bitumen from kerogen. The composition and chemical structure of kerogen is dependent on the solvent that is used for isolation and data is comparable only if the same solvent is used in the extraction.

Isolation of kerogen from the inorganic matter generally requires chemical destruction of the associated inorganic minerals using acid demineralization (Suleimenova et al. 2014) This is performed on the whole rock, prior to or after organic solvent extraction. In both

cases, an additional extraction step is needed after mineral destruction, since hydrogen bonds are broken, or even hydrolysis occur to some extent.

1.3 Kerogen Formation: Diagenesis, Catagenesis, and Metagenesis

The process of kerogen formation begins during senescence of organisms, when the chemical and biological destruction and transformation of organic tissues begin. Kerogen is transformed through three geochemical phases during the burial and compaction of shale: diagenesis, catagenesis and metagenesis (McCarthy et al. 2011). In diagenesis, kerogen loses large amounts of oxygen through the oxidation reactions that liberate gases such as CO_2 and H_2O. Diagenesis ends when humic and fulvic acid amounts in kerogen become insignificant. Some loss of oxygen from kerogen is still observed during catagenesis, particularly for type III kerogen. Following early diagenesis, the transformation of kerogen with depth and generation of hydrocarbons begin. The latter is driven by cracking reactions that are temperature- and time-dependent. H_2O and CO_2 are major products both before and during the main stage of hydrocarbon generation. The end of diagenesis stage to the disappearance of humic acids and not to the end of O/C decrease. Petroleum formation is mainly carried out during catagenesis. Hydrogen and carbon are loss from kerogen. Consequently, H/C atomic ratio of the residual kerogen decreases. There is further loss of CO/CO_2 and that is why O/C atomic ratio continues decreasing at the beginning of the catagenesis stage. During metagenesis, CH_4 is eliminated as well as CO_2, N_2 and H_2S gases (non-hydrocarbon gases).

In 2002, Lorant and Behar (Lorant and Behar 2002) showed that gases are ejected from kerogen using open and close system pyrolysis. CH_4 is formed in two steps, the first one takes place during catagenesis and the second one occurs during metagenesis. In the latter CH_4 occurs with demethylation of methyl aromatics together with cleavage of aromatic ether bridges, yielding gases such as CH_4, CO and CO_2 and some N_2 as observed (Behar et al. 2000). The last step for gas generation is the opening of some aromatic rings. Cleavage of carbon and hydrogen bonds and auto hydrogenation, yielding CH_4 besides CO and CO_2 can be observed for both kerogen and model aromatic compounds during high temperature pyrolysis.

1.4 Methane Generation

In gas shales, the gas is generated in place; the shale is both the source rock and the reservoir. How gas is generated varies from basin to basin and it depends on geological processes. After the deposition of organic-rich sediments, microbial process converts organic matter to biogenic methane gas. As maturation increases, wet gas is generated in late catagenesis and dry gas is also generated in metagenesis. Shale gas is stored interstitially within the pore spaces and it can be adsorbed to the surface of organic materials that are within the shale. Gas typically starts to be generated to a vitrinite reflectance of 0.5 %Ro from humic coals, according to field observations (Scott 1993) and pyrolysis experiments (Tang et al. 1996). The end of gas generation in Kerogen type III, occurs to

vitrinite reflectance range between 1.8 and 2.0 %Ro (Saxby et al. 1986). For enough economic accumulations, gas forms accumulations to a range of vitrinite reflectance of 0.8 and 1.0 %Ro, and pyrolysis experiments (Tang et al. 1996)

1.5 Kerogen Porosity

Kerogen has a multi-scale pore network whose pore sizes vary from nanometers to micrometers. These varieties of pores found in kerogen are function of thermal maturity (G. et al. 2010). Organic pores are developed through thermal cracking in kerogen that are generated after the expelling of hydrocarbons from this organic material. The presence of bubble-like pores in this organic material has been interpreted as evidence that these types of pores are formed after secondary cracking of bitumen in the gas window. Heterogeneous pore distribution has been found for example in mature samples from formations such as Marcellus where the pore distribution is a function of organic matter abundance rather than thermal maturity. In general, organic matter porosity is influenced by two factors: (1) organic matter type, and (2) thermal maturity. On the other hand, primary porosity (in immature samples) is carefully analyzed to determine the influence of primary porosity in subsequent pore placement, structure and development. Although pore size of kerogen may vary significantly, the average pore size is small and typically less than 10 nm (Kang et al. 2011). Organic pores are developed through thermal cracking in kerogen that are generated after the expelling of hydrocarbons from this organic material.

5

1.6 Surface Heterogeneities on Organic Walls

In this thesis, we focus on studying how surface heterogeneities influence the gas storage in kerogen. Mainly, we would like to show how nitrogen atoms left on the kerogen structure affect gas storage if these atoms are located at the pore wall surfaces facing the gas molecules. Note that nitrogen could be released as non-hydrocarbon gases during metagenesis. Hence, we hypothesize that nitrogen is present in the structure of kerogen during diagenesis and catagenesis. Previous investigations based on x-ray photoelectron spectroscopy (Patience et al. 1992, Kelemen, 1999 #31) and based on nuclear magnetic resonance spectroscopy (Knicker, Scaroni, and Hatcher 1996, Derenne, 1998 #34)t have shown that nitrogen amount in kerogen decreases with maturity. This could be due to interaction between pyridine structures and residual OH groups in kerogen (Kelemen, Gorbaty, and Kwiatek 1994) as well as liberation. According to Van Krevelen diagram, ratio between carbon/oxygen and carbon/hydrogen decrease with maturation because oxygen is released from kerogen and consumed early in diageneses stage. Hence, in our research there is no point of including an oxygen atom as impurity into the kerogen pore model. We are in particular interested in those stages, when gas is released, which mean catagenesis and metagenesis, when N_2, H_2S are released. So that is why we considered one of these chemical elements present in the kerogen structure. In addition, in a study of the thermal chemistry of nitrogen in kerogen, direct analysis of nitrogen forms before and after laboratory pyrolysis of immature kerogen have clarified the chemical pathways for nitrogen during late stage diagenesis, catagenesis, and early metagenesis of different types of organic

6

matter. In 1999, Kelemen et al. (Kelemen et al. 1999) identified nitrogen in Green River type I and Bakken type II kerogen and he reported that pyrrolic nitrogen is the most abundant form of nitrogen follow by pyridinic, amino and quaternary types.

Various investigations have also been performed to understand, the chemical structure of kerogen. For the classical treatment of the problem and some insight on the organic matter maturation and kerogen composition, the authors recommend Chapter 4 from Tissot and Welte (Tissot B.P. and D.H. 1984). Kerogen is composed mainly of hydrogen and carbon and the amount of these atoms vary depending on the maturity of kerogen and the evolution of the organic matter. Nitrogen, sulfur and oxygen are also found in this hydrocarbon compound and the atomic percentage differs depending on the type of kerogen as well. Physical analysis, such as electron diffraction, show that kerogen is composed of stack of aromatic sheets, similar to a stack of graphene making up graphite (Tissot B.P. and D.H. 1984). Hence, investigators analyzing methane-kerogen interactions develop slit-like model pores (simple model) consisting of two parallel sheets of graphite which is composed of several (typically, three) layers of graphene (Diaz-Campos 2014, Tissot B.P. and D.H. 1984, He and Zhao 2013, Norman and Filinov 1969). Graphene is an atomic sheet made of carbon hexagonal rings, shown in Figure 1a, and holds mysterious mechanical, thermal and electronic qualities which nowadays find many applications in physical sciences and various technologies. In (Norman and Filinov 1969) the authors have identified in between the graphite layers methane that is confined and segregated into phases: adsorbed molecules right by the walls and free fluid molecules in the central portion of the space in between the

7

layers, i.e., the slit-pores. They have also identified phase transition region in between the adsorbed and free molecules. The authors of the previous works reported that the adsorption of methane on graphite does not really depend on the thickness of the graphite wall, but it is really influenced by the surface area of the wall and the surface properties. Recent studies on fluid transport in single-wall carbon nano-tubes have shown that the storage and transport under the subsurface conditions could be dictated by the pore wall surfaces. It is observed that the fluid is progressively more controlled by the walls as the surface/volume ratio of the pore becomes larger. Riewchotisakul and Akkutlu (Riewchotisakul and Akkutlu) have shown that the total mass flux inside the pore could be significantly enhanced due to mobility of the adsorbed molecules. Figure 1 shows the organic surfaces model which are used in quantum mechanical simulations to calculate fluid-wall interaction parameters σ and ε which are needed later on as input parameters during the Monte Carlo calculations in predicting the methane storage in model pores. Atom colors: carbon (brown), hydrogen (yellow), and nitrogen (blue). The literature on the structural defects of graphene includes di-vacancies and Stone Wales defect. The latter has carbon atoms on the graphene sheet re-organized into two pentagons or two heptagons as illustrated in Figure 1b. And the former, are point defects in which two atoms are missing in two of the lattice sites of graphene and, in turn, create a small distortion in its structure, as is shown in Figure 1c.

(a)   (b)

(c)   (d)
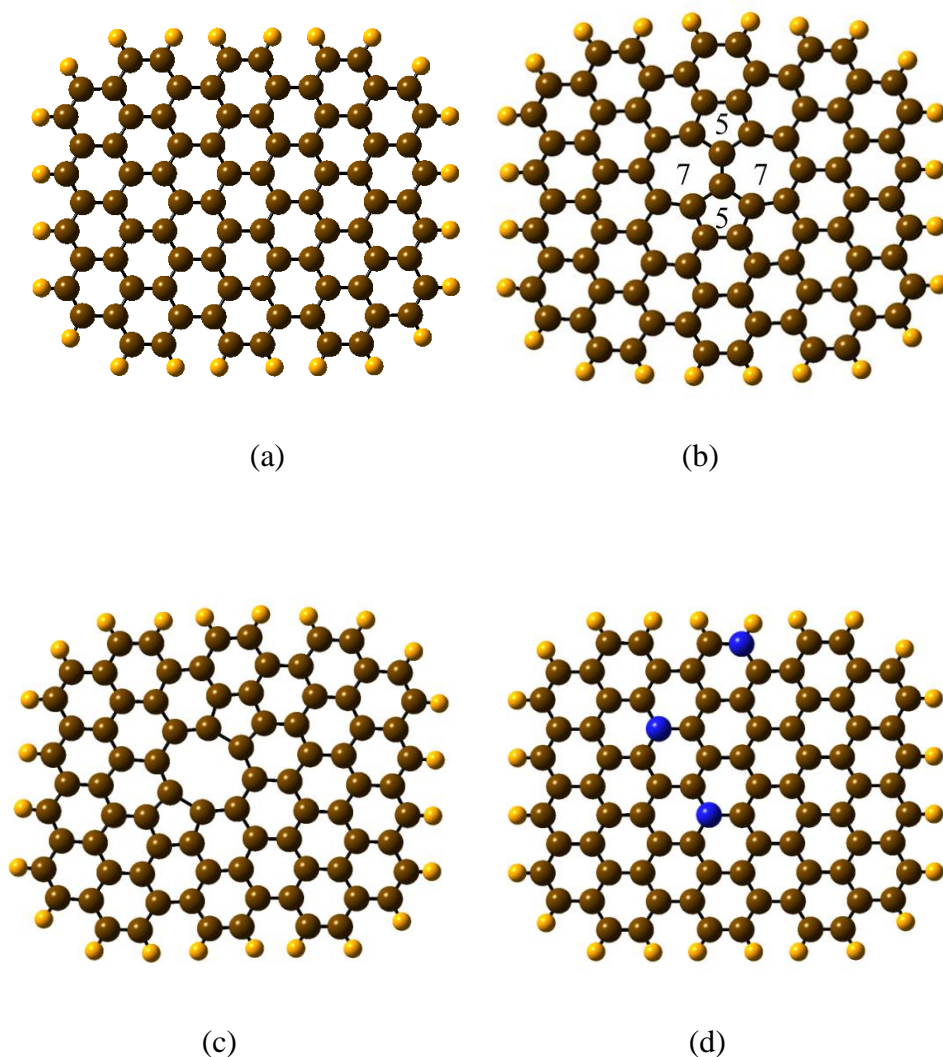
Figure 1. Organic surface models including pristine graphene and the graphene with heterogeneities. (a) pristine graphene, (b) Stone-Wales defect as two pentagons and two heptagons), (c) di-vacancy and (d) N-doping.

The most common kinds of defects found in graphene are vacancies that are produced by breaking the strong covalent bonds between carbons at an energy cost of about 7.8 eV. (Kaxiras and Pandey 1988). Neek-Amal and Shayeganfar found that Van der Waals

interactions between methane and pristine graphene sheet are due to addition of vacancies in the graphene sheet (Shayeganfar and Neek-Amal 2012).

Doping is another graphene defect that takes place when a carbon atom is substituted by another atom such as nitrogen (N) (Figure 1d). The introduction of nitrogen atom into graphene has been effectively confirmed using X-Ray Photoelectron Microscopy (Shao et al. 2010). Wang et al. reported that adsorption of methane on the graphene sheet is enhanced by the insertion of vacancies in the sheet and somewhat influenced by nitrogen doping (Wang Yin et al. 2015).

So far, there are not studies associated that demonstrate how surface heterogeneities influence gas storage in organic nanopores. In previous studies (Ambrose et al. 2012) have investigated multi-scale gas transport in shales with local kerogen heterogeneities, they demonstrated that below a certain critical nanopore size mechanisms such as slippage and hoping lead to molecular streaming by the pore walls which increase the gas transport in kerogen nanopores and also they showed that above this critical pore size gas transport is laminar. In addition, there are not too many investigations using a combination of Monte Carlo and quantum mechanics methods this is why the introduction of this methodology to explore new insights about the gas storage in organic pores at the nanoscale. Only, Ungerer et al. (Ungerer, Collell, and Yiannourakou 2015b) used quantum mechanics and molecular dynamics to predict thermodynamics properties in kerogen, they were able to match experimental values of the kerogen density, they also found that heat capacity increases with

temperature and this behavior is observed non-classical due to the quantization of energy levels. They also reported in their study that standard enthalpy of formation of kerogen changes from negative to positive when maturity goes from low to high. In this study quantum chemistry results are suggested to be used to calculate infrared spectra that are comparable to experimental spectra.

In this thesis, we are interested in identifying the effects of various surface properties on methane adsorption. More specifically, the surface of the most inner graphene sheet will be modified by creating vacancies and by chemically doping it, see Figure 1(d). We are interested in quantifying to what extent the created surface heterogeneities and the structural defects play a role in methane storage in the slit-pore to gain insight into the potential impact of these surface effects on natural.

1.7 Statement of the Problem

Although, several plays of shale gas has been achieved production in U.S., the behavior of the fluid in shale reservoirs is poorly understood because it deviates from conventional reservoir due to the low permeability in the order of nanodarcy, which makes molecular simulation suitable technology to investigate the behavior of shale gas in organic nanopores. Molecular simulation has been implemented in the last years to study the molecular structure, obtain thermodynamic properties, compare simulation with experiment data and determine pore size of particles at the nanoscale. For this reason, in the present document

atomistic modeling and molecular simulation approaches are introduced as a theoretical technique to determine the supercritical methane storage capacity of the organic pores with surface heterogeneities.

1.8 Research Objectives

The current thesis is a document that states research to understand the fluid behavior of supercritical methane in organic nanopores under subsurface conditions. The objectives of the current research are:

(1) Perform a literature review of kerogen to understand its chemical composition and maturation.

(2) Simulate the interaction between methane and graphene and extract Lenard Jones parameters (σ and ε) using atomistic simulations with the help of Gaussian software

(3) Calculate chemical potentials from 0 to 12000 psia of supercritical methane using isothermal isobaric ensemble (NPT) with the help of towhee software.

(4) Model supercritical methane within an organic slit-like pores with sizes from 2 to 5nm using the Grand Canonical Ensemble.

(5) Simulate supercritical methane within an organic slit-like pore with surface heterogeneities.

(6) Estimate density profiles of supercritical methane within an organic slit-like pores

(7) Determine adsorption isotherms methane within an organic slit-like pore

(8) Calculate excess isotherms of supercritical methane within an organic slit-like pores

1.9 Method Overview

A molecular simulation is a technique used in this thesis to simulate the behavior of supercritical methane confined in an organic slit-like pore. These techniques are useful because they can explore the behavior of fluids at nanoscale where experimental techniques are still under development at such a small scale. Two methods are used in the current research; the first one is quantum mechanic methods to simulate the interaction between methane and organic wall at the atomistic level. Second, is the Monte Carlo method where NPT and μVT ensembles are used to determine equilibrium thermodynamic properties. In the Monte Carlo methods different configurations of the fluid are generated that are based on probability distributions. The idea of these calculations is to simulate the fluid until it reaches thermodynamic equilibrium and then count the number of molecules that are accommodate within the pore to observe how the density of supercritical methane is influenced under subsurface conditions, as well as to quantify the amount of gas that is adsorbed and excess of amount of gas that is within an organic pore using Langmuir isotherms; this analysis is important for desorption process for to understand gas production

1.10 Thesis Outline

This thesis is organized in four chapters, the chapter I is about introduction where Shale, kerogen, methane generation, diagenesis, catagenesis, and metagenesis, pore pressure, organic walls and types of pores are discussed. Statement of the problem, research

13

objectives, method overview, and thesis outline are introduced. In chapter II, the methods to calculate the fluid-rock interaction, calculation of chemical potential of bulk methane, pore simulation, and surface roughness are discussed. In chapter III, gas storage in pristine nanopores are argued and in chapter IV gas storage in nanopores with surface heterogeneities are discussed. Finally, chapter V conclusions and future work are introduced.

2. METHODOLOGY

To calculate the storage capacity of kerogen pores at the nanoscale the followed methodology is used: First, fluid-rock interaction is assessed using quantum mechanic calculations; second, chemical potentials of bulk methane is estimated using NPT ensemble and finally the pore is simulated using μVT ensemble. All these methods are explained as follows:

2.1 Fluid-Rock Interaction

The first step is to evaluate the interactions between the fluid and rock. The fluid that is chosen to be modeled is methane and the rock model is an organic wall represented by outer layer of graphite i.e. graphene. The fluid-rock interaction is evaluated using quantum mechanics with the help of Gaussian 09 program (M. J. Frisch 2009). The goal of these calculations is to obtain Lenard-Jones potential curves:

$$LJ = 4\varepsilon \left[\left(\frac{\sigma}{r}\right)^{12} - \left(\frac{\sigma}{r}\right)^{6} \right]$$

Where V_{LJ} is the potential energy, r is the distance between methane and the wall, ε and σ are the L-J parameters. ε is the minimum energy at an equilibrium distance where the attractive and repulsive energies are balanced and represents the strength of the interaction between methane and the carbon of the slit-pore wall. σ is the distance at which the potential energy is zero between methane and the wall. The first term in the equation represents the repulsive term and the second part is the attractive term. The graphic representation of this equation is shown in the Figure 2:
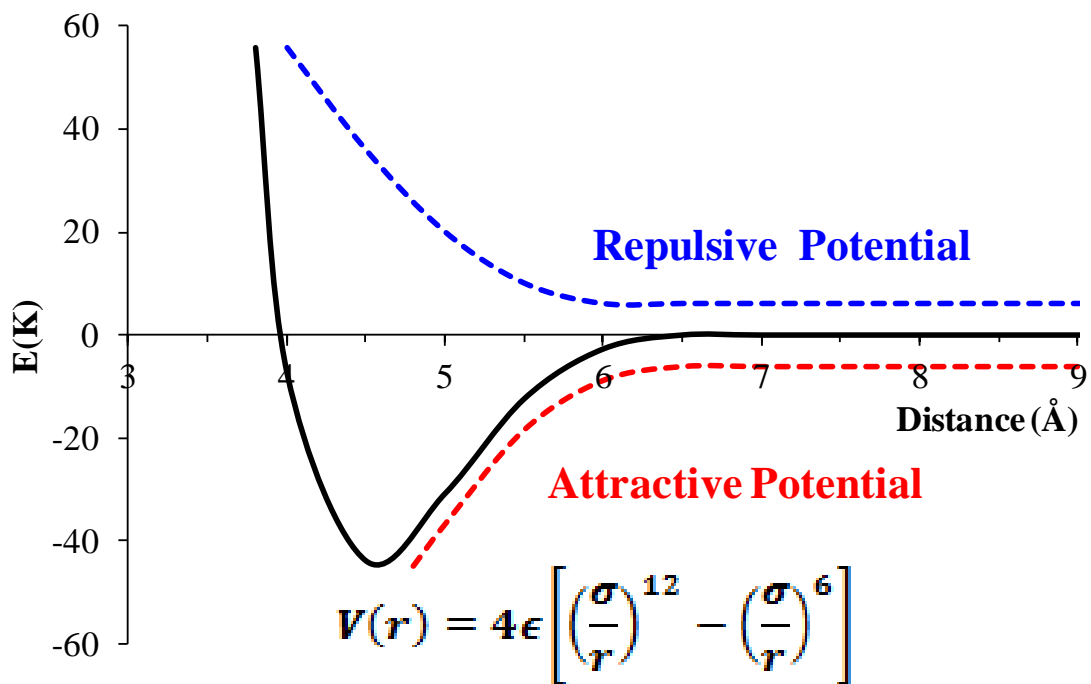
Figure 2. Lenard-Jones Energy Potential representation where the blue lines correspond to the repulsive potential and the red one is the attractive potential.

Optimum values for these parameters can be estimated using MP2 method which uses 6-31(g) basis-set (Ditchfie.R, Hehre, and Pople 1971). This procedure has been tested previously using different level of theory. (Cristancho and Seminario 2010) The MP2 method uses a Hartree-Fock calculation followed by a Møller-Plesset correlation energy correction, truncated at second-order for MP2. Thierfelder C. et al (Thierfelder et al. 2011) has studied the interaction between methane and graphene interaction using (MP2) perturbation theory where they found vales of adsorption energy and molecular distance between methane and organic wall close to the experimental data therefore we based our based fluid-rock interaction using MP2 method.

In these simulations methane and organic wall models (e.g., pristine graphene and graphene with structural defects) are geometrically optimized until they reach energy minima. In the geometry optimization Gaussian uses Berny algorithm which calculates the potential energy and the wave function (probability of finding an electron at given space) of an initial geometry. This procedure is repeated until the algorithm finds a stationary point of the energy where the forces (first derivative of the energy with respect to position) of each atom are zero. Next, several self-consistent calculations of the potential energy (V_{LJ}) is performed between methane molecule and the organic wall model at varying distance (r) values from 3.8 Å to 10 Å. The quantum mechanical simulation and potential energy calculations allow us extract L-J parameters that are needed as input information for the GCMC calculations that would be explained later on in this document.

2.2 Calculation of Chemical Potential of Bulk Methane

Second step of these simulations is to calculate the chemical potential of bulk methane using

Isobaric-Isothermal Ensemble (NPT) simulation which involves a computational box that

has fixed volume and contains bulk methane, i.e., in the absence of pore walls. During NPT

simulation the pressure is fixed to a value in between 500 psi to 12000 psi (McDonald

2002). The total number of molecules (N) and the pore temperature (T) are maintained

constant. The temperature used is 353 K.

The NPT-ensemble average of function is: ((McDonald 2002)

$$\langle f(r^N, v) \rangle = \frac{\int_0^\infty dv\, exp(-\beta pv) \int_v dr^N f(r^N, v) \exp(-\beta \Phi(r^N))}{\int_0^\infty dv\, exp(-\beta pv) \int_v dr^N \exp(-\beta \Phi(r^N))}$$

In these calculations the particles are confined to a cube that is fluctuating edge L:

$$\propto_i = L^{-1} r_i$$

2.3 Pore Simulation

The pore model is simulated as a computational box with two parallel graphite walls that are represented by Steele Wall potential (Steele. 1973) using Towhee software (Martin 2013). The Steele Wall is defined using the following equation:

$$(z) = \varepsilon_w \left[\frac{2}{5} \left(\frac{\sigma_{sf}}{z} \right)^{10} - \left(\frac{\sigma_{sf}}{z} \right)^{4} - \frac{\sigma_{sf}}{[3\Delta(z + 0.61\Delta)^3]}^4 \right]$$

Where

$$\varepsilon_w = 2\pi\varepsilon_{sf}\rho_s\sigma_{sf}^2\Delta$$

The pore is simulated using GCMC simulations, methane is simulated as a spherical site using TraPPE-UA force field (Martin and Siepmann 1998), box is periodic in the x and y directions and fixed to a desired size in the z direction where walls are placed. The slit-pore space is filled with methane molecules; GCMC models the bulk fluid that is in equilibrium by inserting, deleting and displacing molecules. Temperature is 353.15 K and the volume have dimensions of 7.73 nm×7.73 nm in the x and y directions. The pore dimension is increased in the z-direction from 3 to 5nm.

2.3.1 Methane Mass Density

The methane mass density ($\rho_{calc-CH4}$) within the slit-pore for every simulation is calculated using the following equation (Ambrose et al. 2012):

$$\rho_{calc-CH4} = \frac{\rho_{number} M_{CH_4}}{N_A}$$

where N_A is the Avogadro number, M_{CH4} is the molecular weight of methane, ρ_{number} is the number density (number of molecules per volume) of methane. Figure 3 displays a typical isothermal density histogram where adsorbed layer and excess of adsorption can be observed.
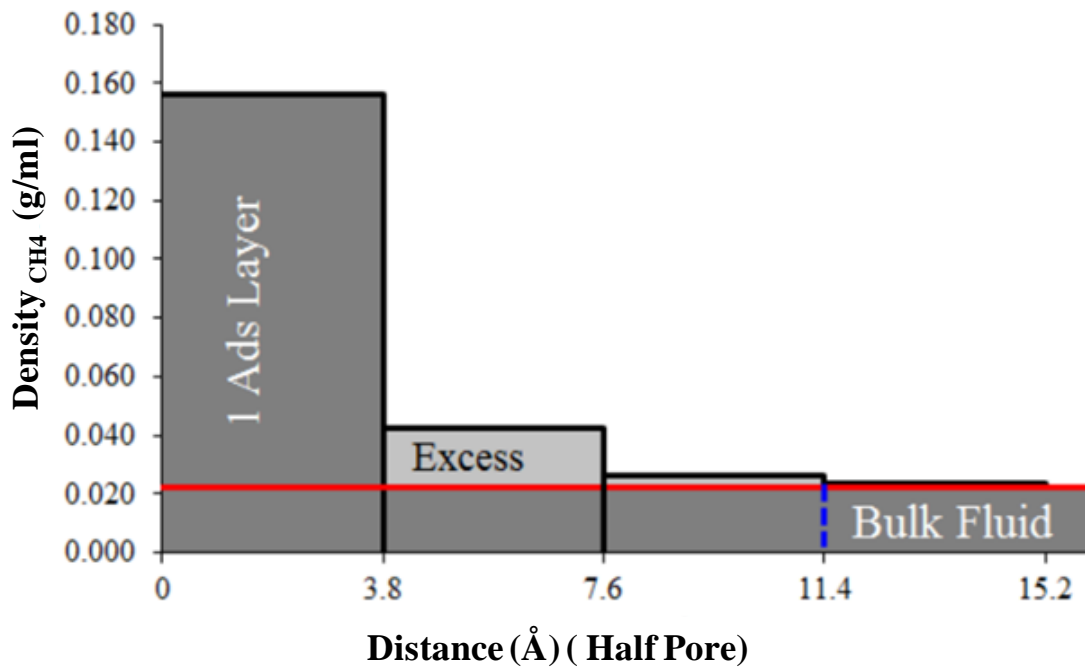
Figure 3. Isothermal density profile of methane between two graphite walls with a separation distance of 4nm at 580 psi. First column: adsorbed layer, light gray columns: excess amount of methane and the last column: bulk fluid (the free gas).

2.3.1.1 Bash code to extract and count values of methane molecules in the pore

After every GCMC simulation, the values of methane molecules are counted and extracted in a excel file to take them to a Matlab Code for plotting. Coding decreases the error in data because several files are extracted in each simulation.

```
catbox_01_step_00000004100000.pdb| awk '{ print $7  }' >      initial0.txt    &
catbox_01_step_00000004200000.pdb| awk '{ print $7  }' >      initial5.txt    &
catbox_01_step_0000000430000.pdb| awk '{ print $7  }' >      initial10.txt   &
catbox_01_step_00000004400000.pdb| awk '{ print $7  }' >      initial15.txt   &
catbox_01_step_00000004500000.pdb| awk '{ print $7  }' >      initial20.txt   &
catbox_01_step_00000004600000.pdb| awk '{ print $7  }' >      initial25.txt   &
catbox_01_step_00000004700000.pdb| awk '{ print $7  }' >      initial30.txt   &
catbox_01_step_00000004800000.pdb| awk '{ print $7  }' >      initial35.txt   &
catbox_01_step_00000004900000.pdb| awk '{ print $7  }' >      initial40.txt   &
catbox_01_step_00000005000000.pdb| awk '{ print $7  }' >      initial45.txt   &
```

/Filter number of molecules by position in the pore

```
for k in `seq 0 5 45`;do
awk '{ if ($1 >= 0.000 && $1 <= 5.475) print $1 }'  initial$k.txt   >     output$k.txt
awk '{ if ($1 >= 5.475 && $1 <= 9.275) print $1 }'  initial$k.txt   >     output$((k+1)).txt
awk '{ if ($1 >= 9.275 && $1 <= 13.075) print $1 }' initial$k.txt   >     output$((k+2)).txt
awk '{ if ($1 >= 13.075 && $1 <= 16.875) print $1 }' initial$k.txt   >   output$((k+3)).txt
awk '{ if ($1 >= 16.875 && $1 <= 20.675) print $1 }'  initial$k.txt  > output$((k+4)).txt
done
```

/Count the number of molecules in pore

```
for i in `seq 0 49`;
do
wc -l output$i.txt      >      count$i.txt
done
```

/Print the number of molecules in the screen

```
for j in `seq 0 49`;
```

```
do

grep ' ' count$j.txt

done
```

2.3.1.2 Matlab code to plot density Values

Density profile of the pore at every bulk fluid pressure is calculated using the following

subroutine in Matlab code:

```
%%%%Matrix that is read from excel file
[A]=xlsread('filename.xlsx')

%%%%%Vectors from every column of the excel file
x=A(:,1)
a=A(:,2)
b=A(:,3)
c=A(:,4)
d=A(:,5)
e=A(:,6)
f=A(:,7)
g=A(:,8)
h=A(:,9)
i=A(:,10)
j=A(:,11)
k=A(:,12)
l=A(:,13)
```

```matlab
%%%%%Plotting
subplot(3,2,1);
plot(x,a,'b',x,g,'r','LineWidth',5);
title('580 psi','FontSize', 22,'FontName','Times New Roman')
xlabel('distance (Å)','FontSize', 22,'FontName','Times New Roman')
ylabel('density(g/ml)','FontSize', 22,'FontName','Times New Roman')
axis([0,38,0,0.4])
set(gca,'xtick',[0,3.8,7.6,11.4,15.2,19.0,22.8,26.6,30.4,34.2,38.0],'FontSize',
20,'FontName','Times New Roman');
set(gca,'ytick',[0,0.1,0.2,0.3,0.4])

subplot(3,2,2);
plot(x,b,'b',x,h,'r','LineWidth',5);
title('2000 psi','FontSize', 22,'FontName','Times New Roman')
xlabel('distance (Å)','FontSize', 22,'FontName','Times New Roman')
ylabel('density(g/ml)','FontSize', 22,'FontName','Times New Roman')
axis([0,38,0,0.4])
set(gca,'xtick',[0,3.8,7.6,11.4,15.2,19.0,22.8,26.6,30.4,34.2,38.0],'FontSize',
20,'FontName','Times New Roman');
set(gca,'ytick',[0,0.1,0.2,0.3,0.4])

subplot(3,2,3);
plot(x,c,'b',x,i,'r','LineWidth',5);
title('4000 psi','FontSize', 22,'FontName','Times New Roman')
xlabel('distance (Å)','FontSize', 22,'FontName','Times New Roman')
ylabel('density(g/ml)','FontSize', 22,'FontName','Times New Roman')
axis([0,38,0,0.4])
```

```matlab
set(gca,'xtick',[0,3.8,7.6,11.4,15.2,19.0,22.8,26.6,30.4,34.2,38.0],'FontSize',
20,'FontName','Times New Roman');
set(gca,'ytick',[0,0.1,0.2,0.3,0.4])

subplot(3,2,4);
plot(x,d,'b',x,j,'r','LineWidth',5);
title('6000 psi','FontSize', 22,'FontName','Times New Roman')
xlabel('distance (Å)','FontSize', 22,'FontName','Times New Roman')
ylabel('density(g/ml)','FontSize', 22,'FontName','Times New Roman')
axis([0,38,0,0.4])
set(gca,'xtick',[0,3.8,7.6,11.4,15.2,19.0,22.8,26.6,30.4,34.2,38.0],'FontSize',
20,'FontName','Times New Roman');
set(gca,'ytick',[0,0.1,0.2,0.3,0.4])

subplot(3,2,5);
plot(x,e,'b',x,k,'r','LineWidth',5);
title('8000 psi','FontSize', 22,'FontName','Times New Roman')
xlabel('distance (Å)','FontSize', 22,'FontName','Times New Roman')
ylabel('density(g/ml)','FontSize', 22,'FontName','Times New Roman')
axis([0,38,0,0.4])
set(gca,'xtick',[0,3.8,7.6,11.4,15.2,19.0,22.8,26.6,30.4,34.2,38.0],'FontSize',
20,'FontName','Times New Roman');
set(gca,'ytick',[0,0.1,0.2,0.3,0.4])

subplot(3,2,6);
plot(x,f,'b',x,l,'r','LineWidth',5);
title('12000 psi','FontSize', 22,'FontName','Times New Roman')
xlabel('distance (Å)','FontSize', 22,'FontName','Times New Roman')
```

ylabel('density(g/ml)','FontSize', 22,'FontName','Times New Roman')

axis([0,38,0,0.4])

set(gca,'xtick',[0,3.8,7.6,11.4,15.2,19.0,22.8,26.6,30.4,34.2,38.0],'FontSize',

20,'FontName','Times New Roman');

set(gca,'ytick',[0,0.1,0.2,0.3,0.4])

2.3.2 Langmuir Adsorption Isotherm

The distribution of methane in the pore is characterized using a storage model such as

Langmuir, based on the mono-layer assumption; one would take into account the molecules

in the first layer as the adsorbed amount. Based on the adsorption theory on flat surface and

in pores, the adsorbed methane rises linearly at low pressure and reaches saturation at high

pressure. Hence, a nonlinear methane adsorption isotherm is expected as is shown in Figure

4.
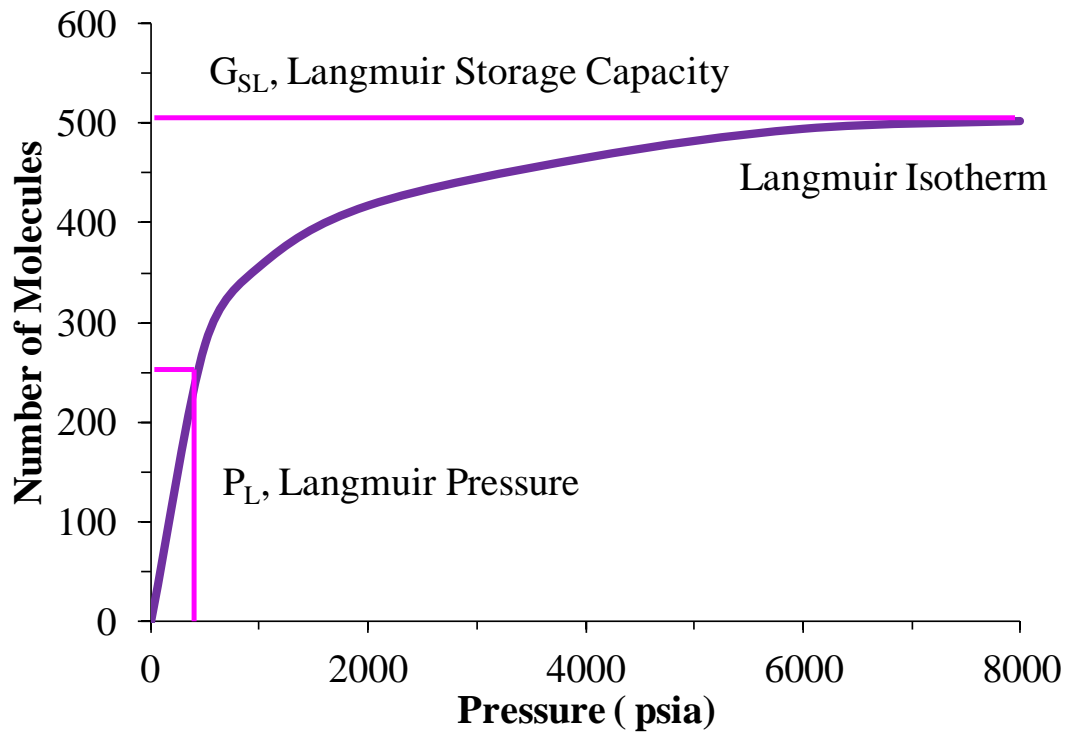
Figure 4. Langmuir Isotherm for monolayer adsorption model. G_{SL} is the Langmuir storage capacity in moles and P_L is the Langmuir pressure in psi.

2.3.3 Excess Absorption Isotherm

Excess amount of adsorption, on the other hand, can be calculated using:

$$n_{excess} = \frac{\left[\sum_{i=2}^{N}(\rho_{calc-CH4} - \rho_{bulk-CH4})V_{3.8}\right] * N_A}{M_{CH_4}}$$

where n_{excess} is the mass of excess methane molecules, ρ_{bulk} is the mass bulk density of methane from NIST, standards and Technology (NIST 2011), $V_{3.8}$ is a volume segment within the slit-pore. Each segment has size in the z direction is 3.8 Å which correspond to the diameter of methane molecules. In Figure 5 is shown the flowchart that is used to perform the current research.
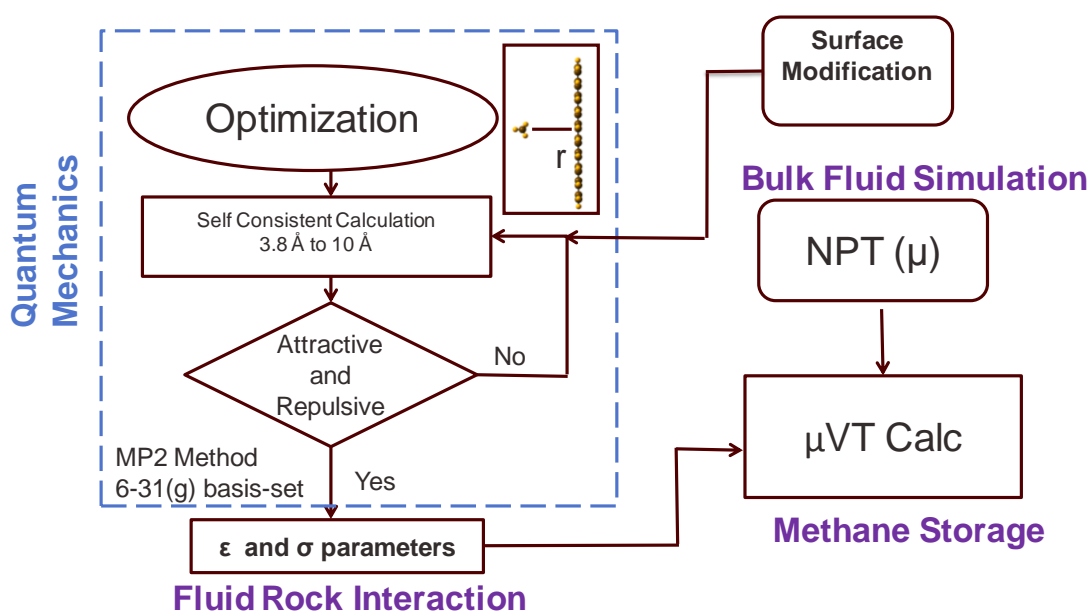
Figure 5. Flowchart used in the current research to investigate the simulation of methane confined in organic nanopores.

3. GAS STORAGE IN PRISTINE NANOPORES

3.1 Chemical Potential of Bulk Methane

Figure 6 shows the computed chemical potential of bulk methane versus pressure. The form of the predicted curve follows the regular shape for simple gases. The chemical potential increases as the pressure increases; at low pressures, the activity (chemical potential) of CH_4 molecules are significantly influenced by the pressure; however, at higher pressures, the dependence is somewhat less influenced making the slope of the curve decline and becomes constant. The chemical potential value at a particular fluid pressure in Figure 6 is used as input for the GCMC calculations.

Figure 6. Chemical potential dependence of methane with varying fluid pressure.

3.2 The Effect of Nano-pore Confinement on Gas Adsorption

To understand the effect of nanopore confinement on methane adsorption, we used model slit-pores with pristine walls first. GCMC simulation gives numerically predicted methane adsorption isotherm and excess methane amounts. Note that the adsorbed amount is based on the accumulated molecules within the first layer by the wall, whereas the excess amounts are based on the number of methane molecules within the inner segments.
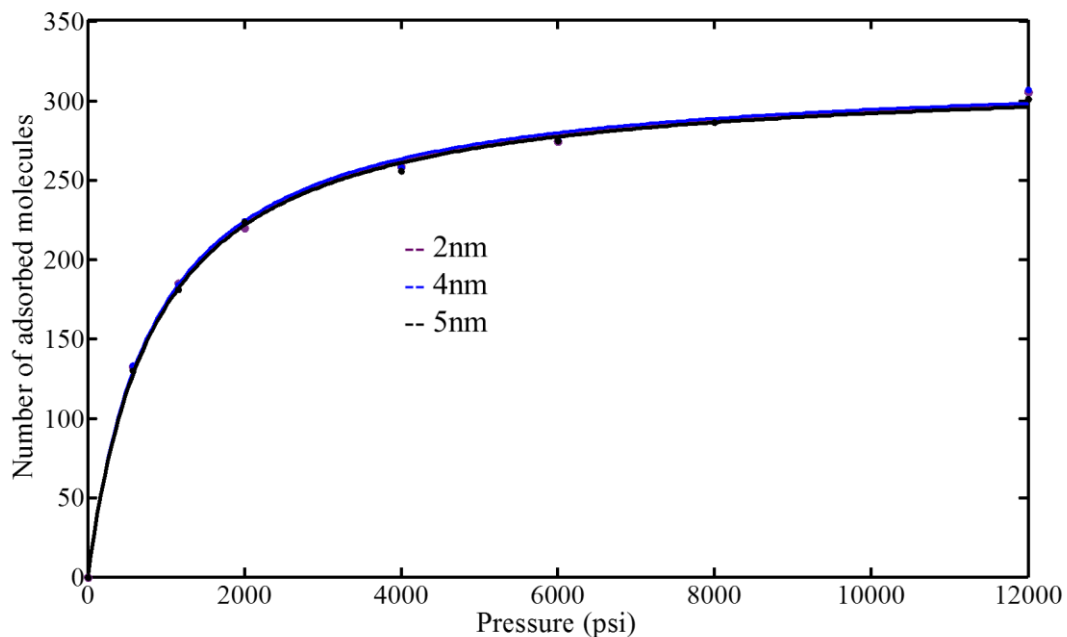
Figure 7. Langmuir adsorption isotherms for methane in slit-shape pores with sizes 2, 4 and 5nm.The pore walls are made of pristine graphene, i.e., no surface heterogeneities. Natural gas in place calculations are currently performed using Langmuir model, which is the most widely used model in the petroleum industry. This model is used to quantify the

first-layer of adsorbed amount in Kerogen organic nanopores with slit-like shape and in essence show the BET-like behavior of the supercritical methane adsorption in nanopores with thicknesses of the pores as 2nm, 4nm, and 5nm. As shown in Figure 7, no variation exists in the adsorbed amount as the size of the pore is changed from 2 nm to 5 nm. This indicates that the increasing level of confinement does not influence the adsorbed molecules in the first layer because the adsorbed amount is dependent in the surface area which is kept constant.
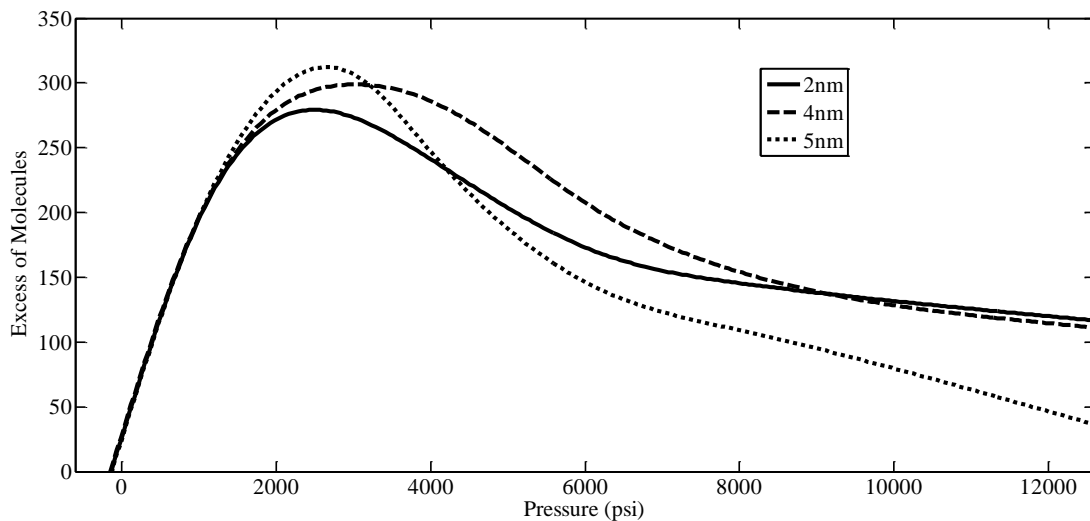
Figure 8. Excess amount of methane in slit-shape nanopores with varying sizes.

The estimated excess amount, on the other hand, is shown in Figure 8. Note that the excess amount is significantly influenced by the fluid (or pore) pressure. There exists a range of pressure in between 1,000psi to 5,000psi where the excess amount is comparatively quite high. Clearly the confinement plays a significant role in methane storage under the

subsurface conditions. At the extreme conditions of pressure the excess amount contribution is relatively less. Note that no significant variation due to nano-pore size because the surface area is mantained constant , as is observed in the excess amount either since the fluid behavior is quite consistent in the nanopores

3.3 Isothermal Methane Density Profile

Figure 9 shows the isothermal density profile of methane across the width of a 4nm slit-shape pore with pristine graphene walls. The simulations show that the density of methane is not uniform but has a structure across the pore. Methane molecules are adsorbed on the graphene surface forming an adsorbed layer and then a staircase structure appears involving several layers of methane molecules as the center of the pore is approached. This observation has been reported before in other studies, see for example (Ambrose et al. 2012). Adsorbed methane on the pore wall is observed within the volume segment from 0 to 3.8 Å, i.e., the first layer of methane, where methane molecules are under the strong influence of the Van der Waals forces imposed by the wall. Hence, methane density is the highest in this first layer. The methane density near the wall is high because the attractive forces between the wall and methane molecules are much greater in magnitude than the attractive forces between the methane-methane molecules. The attractive forces become less away from the wall, thereby the density decreases as the distance of gas molecules increases with respect to the wall. There are two walls in a slit-shaped pore thus the density decreases until the pore half-length and then increases symmetrically until it reaches the second wall.
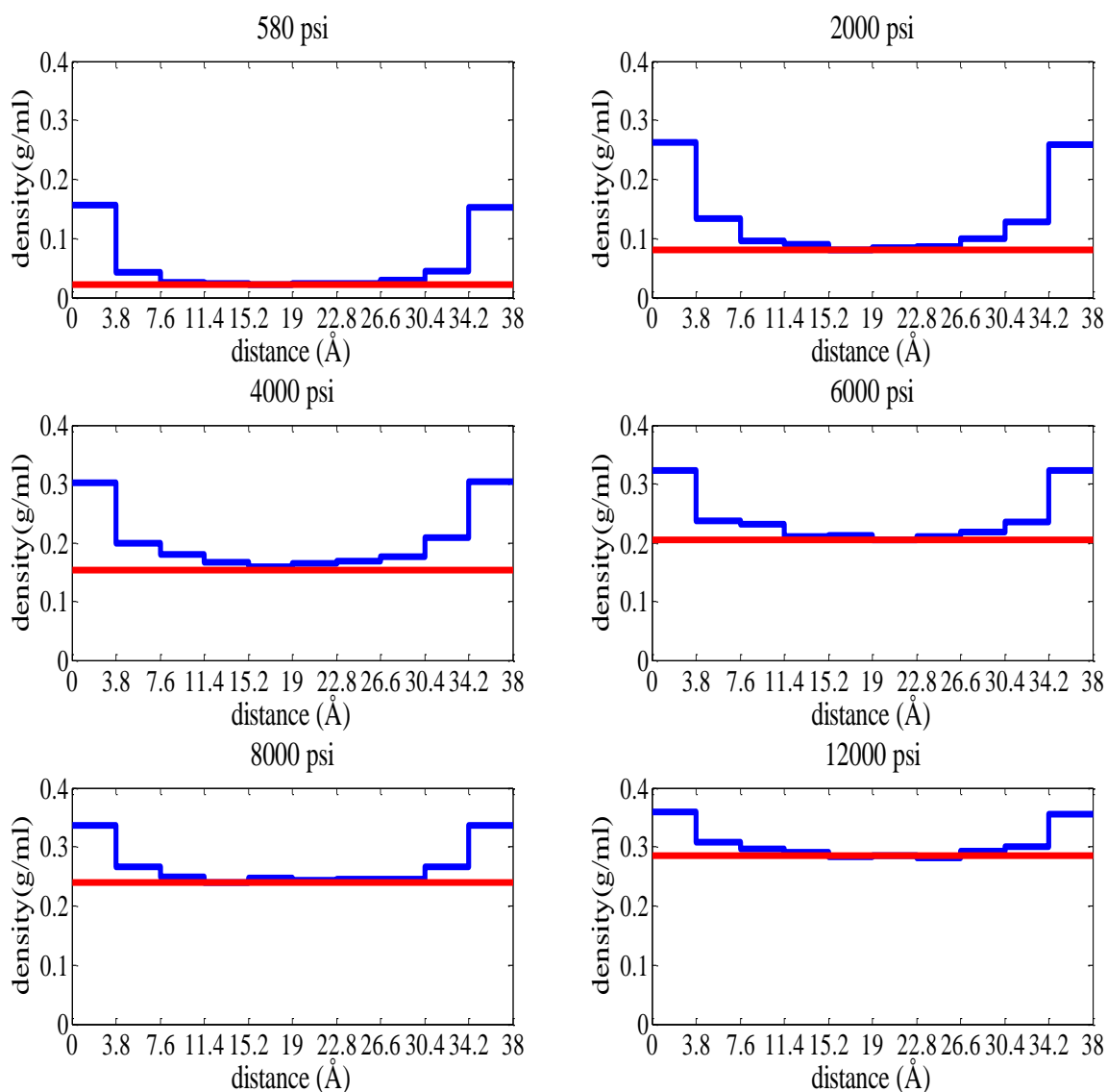
Figure 9. Density of methane across a 4nm slit pore with pristine walls at 353K.

Also note that the density of the first adsorption layer increases linearly at moderate pressures, and is stabilized because the surface reaches saturation at high pressure. In addition, the density matches the bulk value in the center of the pore and this is called the free gas in pore. (Didar Behnaz and Yucel. 2013)

4. GAS STORAGE IN DEFECTED NANOPORES

4.1 Gas Adsorption in Nanopores with Surface Heterogeneties

Interactions between methane and graphene walls with varying surface properties are investigated next through the potential energy functions as displayed in Figure 10. These energy functions are based on the quantum calculations and represent the interplay between the repulsive and attractive energies between methane and the wall molecules. From these curves parameters σ and ε are calculated for various solid surfaces: pristine graphene, Nitrogen-doped graphene and graphene with vacancies, i.e., di-vacancy and Stone-Wales. The estimated parameter values are given in Table 1. The level of variability in the interactions can be seen through the estimated ε values in Table 1. ε slightly varies in the range of 44 K to 49.2 K with the heterogeneities. Consequently, it is found that the impact of surface heterogeneities is not significant on the predicted potential energy function. From this observation we can conclude that the roughness of the wall do not play any role in the adsorption of gas molecules because of the weak interaction between the fluid and the roughness.

Figure 10. Lenard-Jones potential energy for the interaction between methane and various walls: graphene, N-doped, di-vacancy and Stone-Wales.

In large pores, since the adsorbed amount of methane is independent of the variation of the pore width and primarily dependent on the graphite surface area, in this section of the report we decided to fix the pore width to 4nm and focus on the effects of the surface heterogeneities. The surface area is also fixed. The calculated adsorption isotherms and the excess amounts changing with surface heterogeneities are shown in Figures 11 and 12, respectively. There is no significant variation in the isotherms and the excess amounts when heterogeneities are present on the surface of graphene. This is due to weak physical interaction of methane and the walls, as described by Lenard-Jones potential. In the following pages we focus to the nitrogen doping effect on the storage.
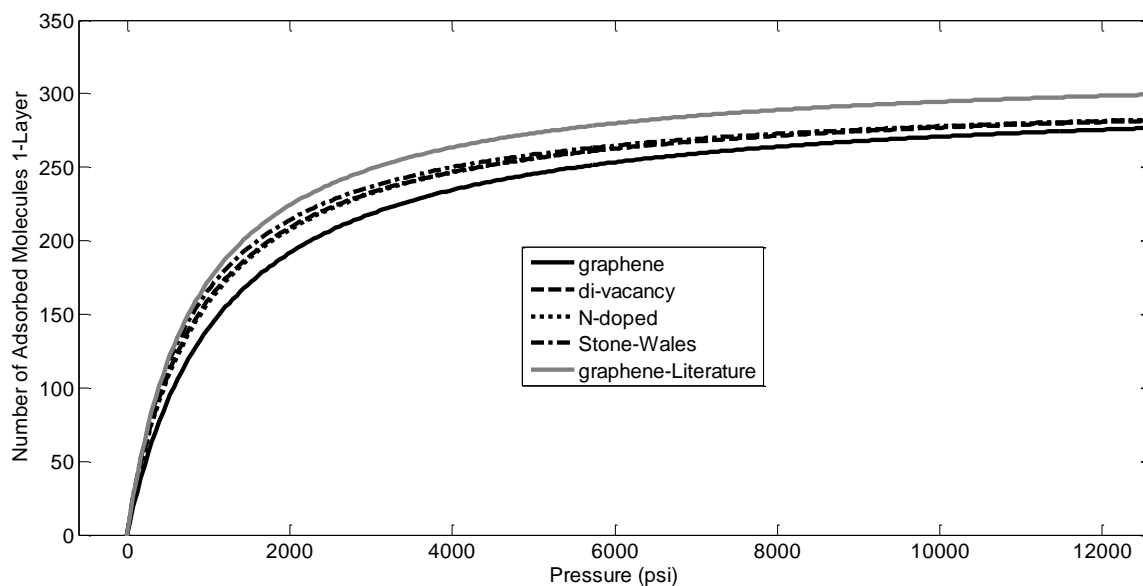
Figure 11. Adsorption isotherms for methane in 4nm graphene pore with heterogeneities on the surface.
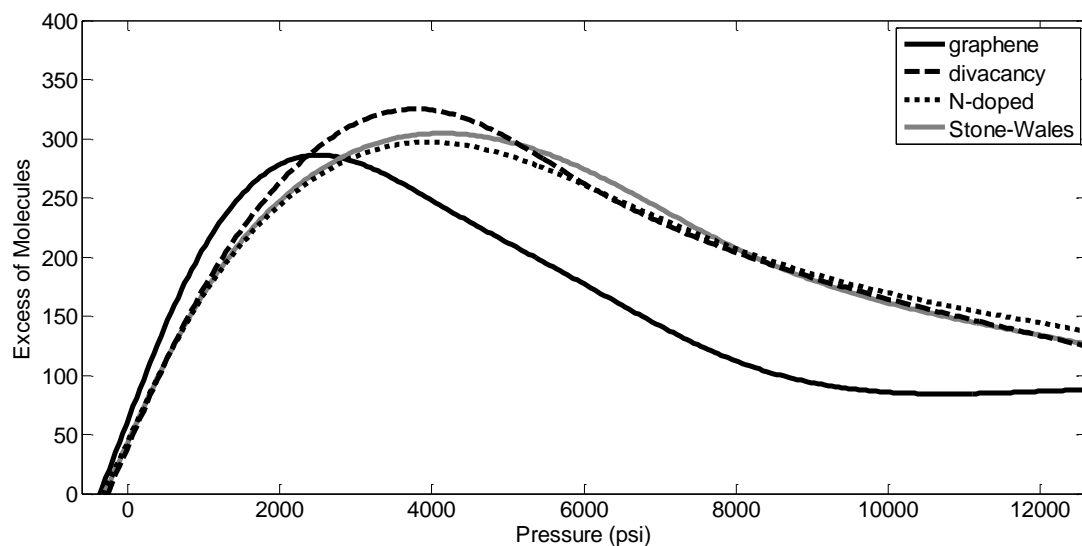
Figure 12. Excess adsorption of methane in slit-pore with surface heterogeneities. The excess amount calculations exclude the first layer of adsorption by the walls.

Table 1. Lenard-Jones parameters of methane-graphite interactions in presence of

heterogeneities.

Model	$\varepsilon(K)$	$\sigma(nm)$
Graphene*	-44.00	0.395
di-vacancy	-46.78	0.400
N-doped	-48.32	0.390
Stone-wales	-49.18	0.392

4.2 N-doping Effect on Gas Adsorption in Nanopores

In order to find out what actually influence the gas storage, which ultimately will affect the

calculation of gas in place, the concentration of nitrogen atoms is varied on the surface of

the pore from one, to two and three nitrogen atoms to see the effect in the gas storage. The

rationale behind this approach is because if this investigation would have been done

experimentally using scanning electron microscopy, this technique would have been able to

scan the surface of the pore therefore it would have been possible to find irregularities that

distorts the density of states between the tip of a STM and the surface. Therefore, the initial

guess is to increase the number of inorganic impurities found in kerogen such as nitrogen on

the surface. Among the heterogeneities investigated, nitrogen-doping is found to be the most

influential on the fluid-solid interactions. This effect becomes more pronounced when the

number of nitrogen atoms available at the surface is increased.

Figure 13 shows the estimated adsorption isotherms of methane on a 4 nm carbon slit-pore with varying nitrogen concentration at the pore walls. These results clearly show that the adsorption amount of methane on a carbon slit-pore is strongly dependent on the nitrogen concentration at the wall. 33.7 % increase of adsorbed amount of methane is recorded when N-doping decreases from 3N to 2N on the surface at 2000 psi. 63.5 % increase of adsorbed methane is recorded when N-doping decreases from 3N to 1N on the surface at 2000 psi. These results suggest that nitrogen on the surface of an organic slit-like pore model has a prominent effect on the adsorbed gas amount in the pore. The surface of pristine graphite has delocalized π electrons which are created from the overlapping of the lobes of the p orbitals; (Cristancho 2014) however, when we introduce impurities on the graphene sheet, a redistribution of the π electrons takes place when more than one nitrogen atom is added on the surface of graphene, certainly the surface of graphite becomes n-type so there would be a reorganized cloud of free electrons on the surface that weakens the Van der Waals interaction between methane and the surface; consequently, the adsorbed gas amount decreases as the number of nitrogen atoms increases on the surface.
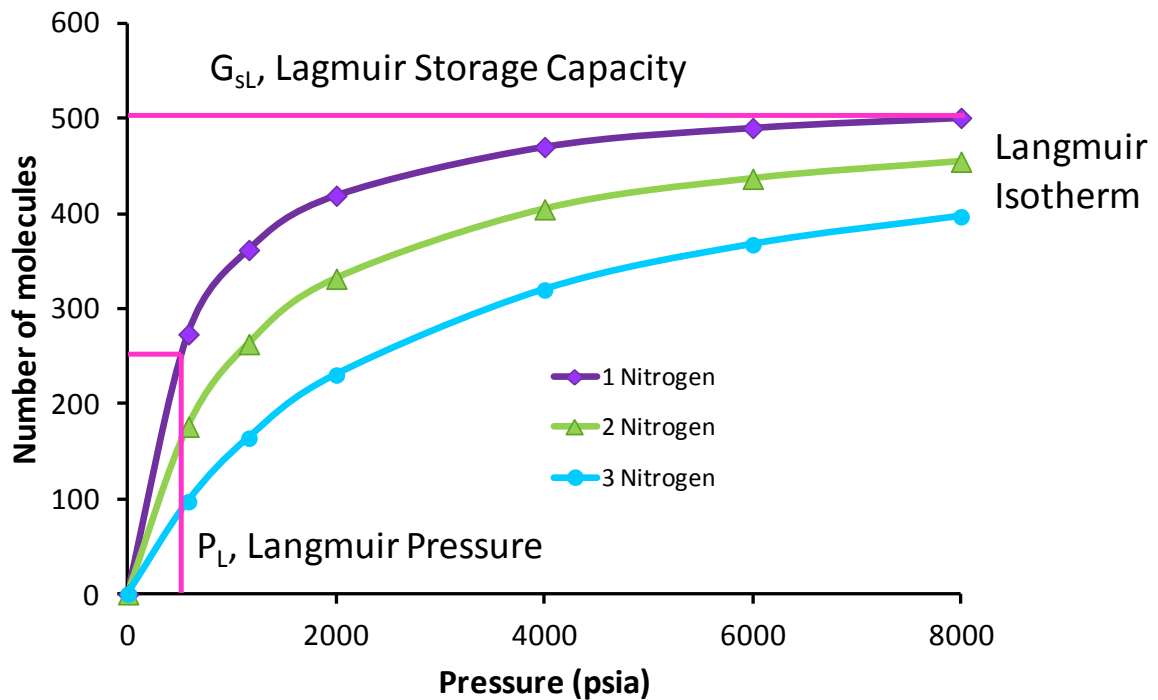
Figure 13. Adsorption isotherms in a slit-pore of 4nm with nitrogen doping, varying the concentration of nitrogen from 1 to 3 atoms on the surface.

The results are important because nitrogen is found in the structure of kerogen in shale and it decreases during metagenesis. In 2007, ExxonMobil (Kelemen et al. 2007) demonstrated that nitrogen compound exists as pyrrolic forms in all kerogens that they studied. Later, Ungerer et al. (Ungerer, Collell, and Yiannourakou 2015a) shown that kerogen II-C and kerogen II-D models are potential for gas generation and their structures contain nitrogen atoms. Nitrogen is lost primarily during late catagenesis or early metagenesis, after hydrogen loss has advanced. N_2 gas is the only nitrogen-containing gas generated from kerogen and it is almost exclusively formed during metagenesis (Behar et al. 1998). In

essence, our results are indicating what the consequences on the gas storage are when the concentration of impurities such as nitrogen vary in the structure of kerogen models during metagenesis. When kerogen becomes more graphitic (aromatic), the maximum adsorbed amount of methane in the pore, G_{sL}, increase significantly. G_{sL} is the asymptote at high pressures of Lagmuir isotherms as shown in Figure 13.

When the pore pressure in the shale formation is reduced down to the Langmuir pressure, for example, nearly half of the gas is desorbed from the pores with 1 nitrogen surface. Langmuir pressure would it be in this case the BHP (bottom hole pressure) when gas is produced and the rate of the curvature is defined as the slope between the delta of storage capacity (mol) divided by the delta of pore pressure. If desorption occurs, it started an initial presure Pi and the difference between P_i and $P=P_L$ would it be the pressure drawdown that drives the gas outs from the reservoir into the wellbore when drilling (horizontal and vertical), completion, and well stimulation have done it.

The Langmuir model parameters are predicted by fitting the isotherms shown in Figure 13. Notice that the total amount of adsorbed amount correspond to the total amount of gas that is adsorbed in both graphite sheets in an organic slit-like pore. In the process of curve-fitting, the following equation has been used: (Ambrose, 2012)

$$G_a = G_{sL}\frac{p}{p + p_L}$$

Where G_a is the surface component and represents the amount of gas that is physically adsorbed on the surface of micropores and mesopores. Lagmuir storage capacity, G_{sL}, is given in moles representing the maximum adsorbed amount of methane in the pore and is the slope in the surface component equation. The Lagmuir pressure, on the other hand, is given in psi. The estimated parameters are converted to practical units and tabulated in Table 2.

Table 2 Predicted Langmuir parameters for methane adsorption in 4nm pore with graphite walls.

Number of Nitrogen on the Surface	G_{sL} (mol)	p_L (psi)
1	536	557
2	519	1129
3	523	2536

Note that G_{sL} is not too sensitive to N-doping but the Langmuir pressure is extremely sensitive to the surface roughness due to nitrogen. As the number of nitrogen increases, P_L increases therefore the pressure drawdown (P- P_L) decreases for the same initial reservoir pressure and therefore the gas rate in reservoir production. However, research is undergoing at the nanoscale to understand the fluid-flow behavior and transport of shale gas because in

the nanopores non-Darcy flow occurs which deviates from conventional reservoirs. (Swami, Clarkson, and Settari).
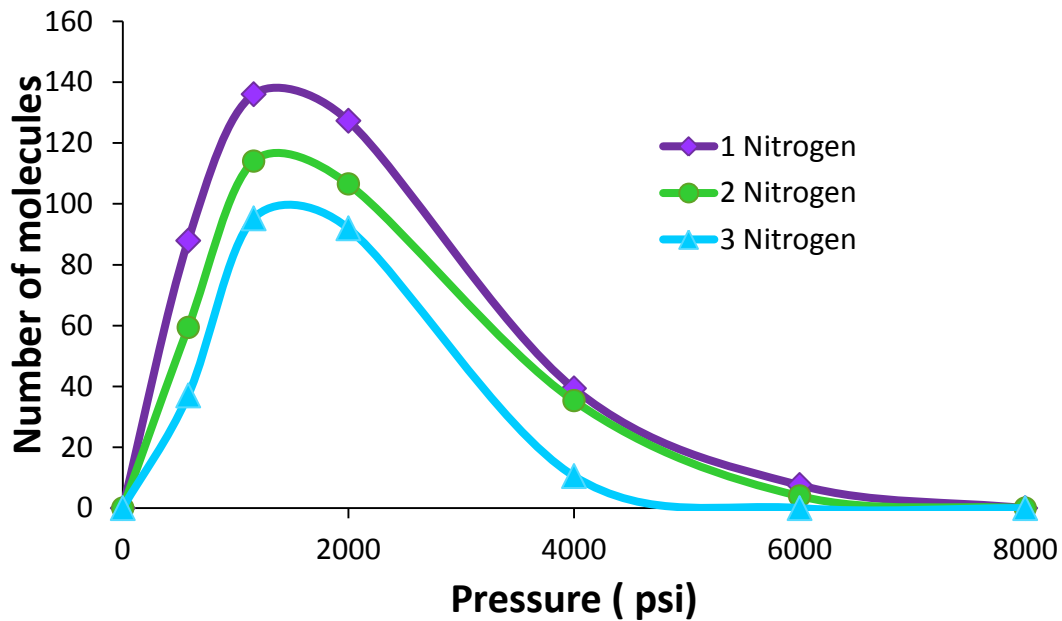
Figure 14. Excess adsorption of methane in a slit-pore of 4nm with nitrogen doping, the concentration of nitrogen varies from 1 to 3 nitrogen atoms on the surface.

According to the predicted behaviour in Figure 13, when the pressure decreases, the adsorbed methane desorb non-linearly as the reservoir is depleted. In addition, when the pressures declines until the Lagmuir pressure, half of the shale gas is desorbed from the pore; therefore, shale nanopores from the dry gas window will desorb higher amounts of adsorbed gas than the ones from wet gas window. The remaining amount of gas will be desorbed when pressures declines less than Lagmuir pressure.
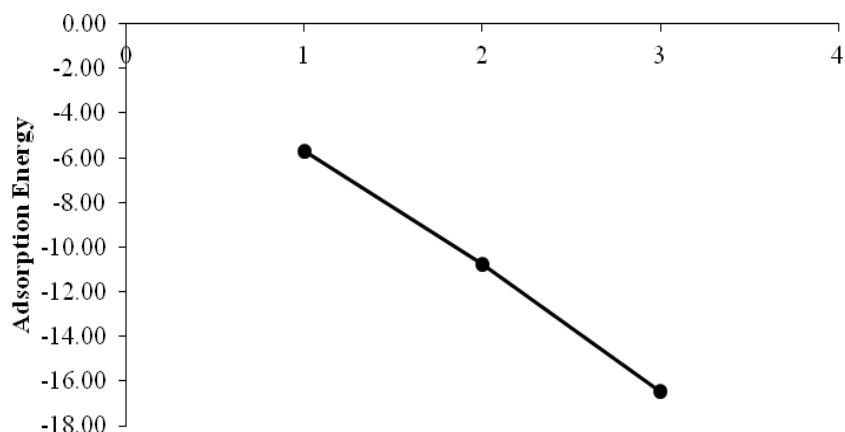
Figure 15. Calculated adsorption energies for methane-graphene wall interactions with changing number of nitrogen atoms on the surface.

The estimated excess amount of methane is also nitrogen-doping dependent as is shown in Figure 14. There is an increase of excess amount in 15.8% when nitrogen concentration is decreased from 2N to 3N at 2000 psi. Increase of excess amount is 38.42% when the concentration is decreased from 1N to 3N on at the same pressure. The increase in excess amount of gas in carbon-slit pore with nitrogen on the surface is explained through the Lenard-Jones potential curves in Figure 17. When two nitrogen atoms exist on the solid surface, the depth of the potential is less than that when there is one nitrogen on the surface. Hence, van der Waals interactions become weaker as the number of nitrogens on the surface increases, the weaker the Van de Waals interactions, the less excess amount of gas that experienced the forces imposed from the surface wall, we can treat this phenomena as an immiscibility that exist from organic and inorganic constituents in the source rock between nitrogen and methane, the less nitrogen on the surface, the more excess gas that is attracted

44

on the surface of the pore. Figure 16 shows the total amount of storage gas in the pore, adsorbed plus excess amount and the form of the curve.
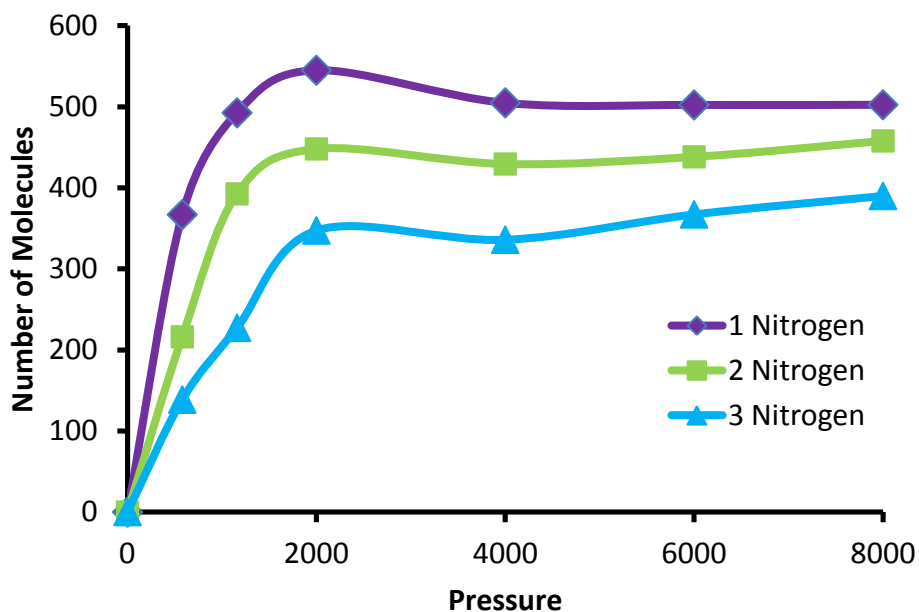
Figure 16. Total (adsorbed plus excess) amount of gas storage in a 4nm nano-pore with nitrogen doping. The concentration of nitrogen varies from 1 to 3 nitrogen atoms on the surface.

Figure 15 shows that the level of methane-wall interactions is reduced by a factor of 3 when the number of doped nitrogen on the pore walls is increased from one to three. In essence, the more nitrogen present, the less adsorption pore walls experience. To reduce computational cost, ε data for graphene with three nitrogen atoms was calculated by extrapolating the value for the cases with 1 and 2 nitrogen atoms as is shown in Figure 16. Assuming the relationship between ε and the number of nitrogen on the organic surface

linear, it decreases as the number of nitrogen atoms on the organic surface increases. These

are shown in Table 3
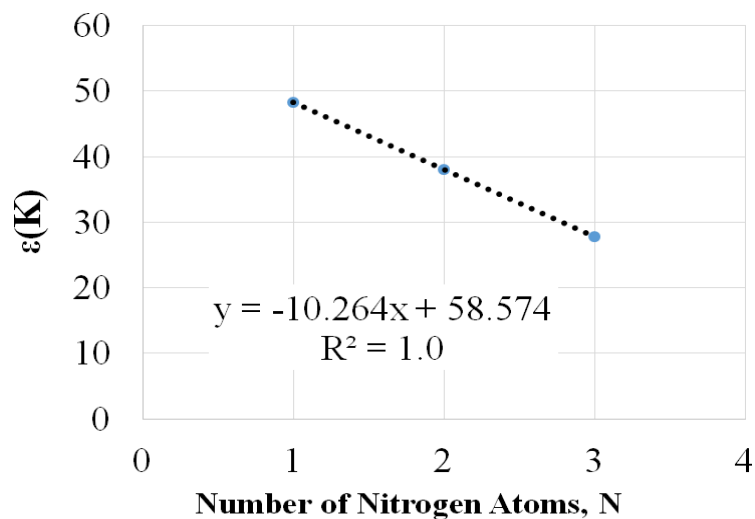
Figure 17. Epsilon versus number of nitrogen on the organic surface.

Table 3 Epsilon and sigma interaction parameters between methane and organic surfaces

with 1, 2, and 3 nitrogen atoms as predicted using quantum mechanical calculations and

linear extrapolation.

N	ε (K)	σ (nm)
1	48.31	3.9
2	38.05	3.9
3	27.78	3.9
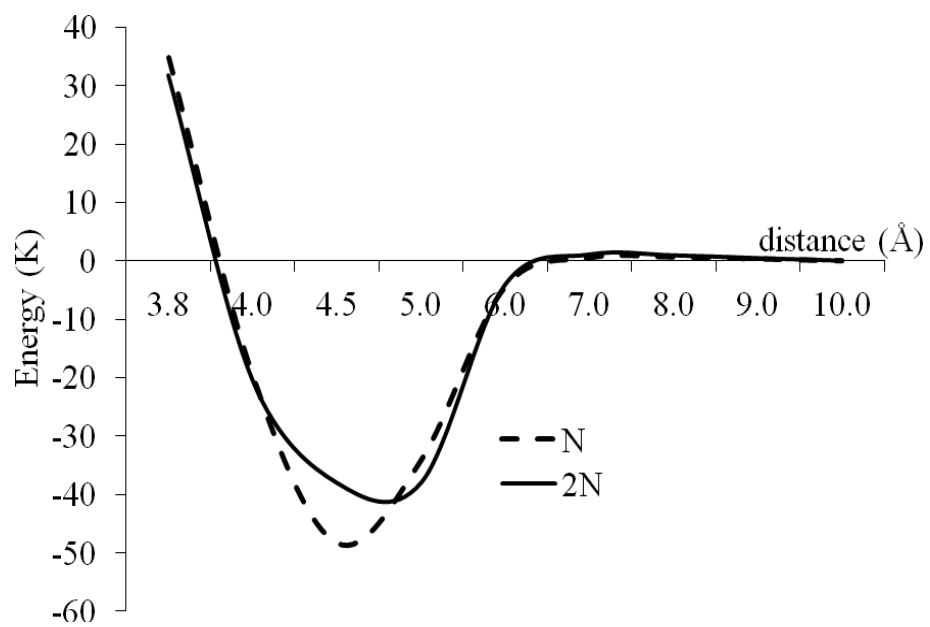
Figure 18. Lenard-Jones Potential for graphene doped with 1 and 2 nitrogen atoms.

5. CONCLUSION AND FUTURE WORK

The adsorption of methane in nano-scale organic pores is sensitive to the surface area available for adsorption but independent of the size of the pore. The excess amount due to confinement effect is most pronounced under the subsurface conditions where the pressure is in the range of 1,000-5,000 psi. The surface heterogeneities have the potential to impact methane adsorption depending on the level of heterogeneities. In this study, based on the geochemical arguments that have been made previously, we showed the sensitivity to nitrogen-doping. The molecular simulation results clearly show the influence of doping is pronounced on the fluid storage.

The surface roughness is geochemistry-dependent and in this paper we identified this dependence using adsorption isotherm and excess amount data. As the concentration of nitrogen on the pore wall surface increases, the isotherms indicate a significantly less storage capacity. Based on the arguments on the nature of non-hydrocarbon gas release during metagenesis, shale gas reservoirs that are in the dry gas window could be exposed to such storage effects. We finally conclude that the gas in place calculation of Shale gas for reservoirs with porosity at the nanoscale is dependent of the surface area and surface chemistry of the pores and the percentage content of inorganic compounds like nitrogen in the chemical structure of source organic material: Kerogen.

6. RECOMMENDATIONS

Geochemistry plays a role in the adsorption and desorption of gas in kerogen pores; therefore, it is recommended to test other chemical elements found in mature kerogen such as sulfur. The current study simulates how Shale gas is storage as gas in place in kerogen source rock with porosity at the nanoscale with the loss of N_2 non-hydrocarbon components.

Graphitic slit-like pores are an approximated model of the nanopores because underestimate the gas is in place calculation; therefore, it is recommended to simulate kerogen as 3-D material where the percentage of non-hydrocarbon is taking into account in the molecular structure of kerogen. Shale gas for exploration has to be in metagenesis where non-hydrocarbons are released.

REFERENCES

Alexander, Tom., Jason. Baihly, Chuck. Boyer et al. 2011. Shale Gas Revolution. *Oilfield Review* **23** (3): 40-55.

Ambrose, Ray J., Robert C. Hartman, Mery Diaz-Campos et al. 2012. Shale Gas-in-Place Calculations Part I: New Pore-Scale Considerations. *Spe Journal* **17** (1): 219-229.

Behar, F., B. Gillaizeau, S. Derenne et al. 1998. Nitrogen Fate During Laboratory Maturation of Two Kerogens (type I and type III). Implications for Nitrogen cycle. Proc., Goldschmidt Conference Toulouse.

Behar, F., B. Gillaizeau, S. Derenne et al. 2000. Nitrogen Distribution in the Pyrolysis Products of a Type II Kerogen (Cenomanian, Italy). Timing of Molecular Nitrogen Production versus Other Gases. *Energy & Fuels* **14** (2): 431-440.

Cristancho, D. 2014. Ab Initio Study of Nanostructures For Energy Storage. Master of Science in MSEN, Texas A&M University, College Station, TX (May 2014).

Cristancho, D., J. M. Seminario. 2010. Polypeptides in alpha-helix conformation perform as diodes. *Journal of Chemical Physics* **132** (6). 065102.

Diaz-Campos, Mery. 2014. A Novel Approach for Reservoir Simulation and Fluid Characterization of Unconventional Fields: Phase 1 Molecular Level Considerations. *SPE*.

Didar Behnaz, Akkutlu I. Yucel. 2013. Pore-size Dependence of Fluid Phase Behavior and Properties in Organic-Rich Shale Reservoirs. Proc., SPE International Symposium on Oilfield Chemistry, The Woodlands, Texas, USA.

Ditchfie.R, W. J. Hehre, J. A. Pople. 1971. Self-Consistent Molecular-Orbital Methods .9. Extended Gaussian-Type Basis for Molecular-Orbital Studies of Organic Molecules. *Journal of Chemical Physics* **54** (2): 724-&.

Durand. 1980. *Sedimentary organic matter and kerogen. Definition and quantitative importance of kerogen* (Reprint).

G., Loucks Robert, Reed Robert M., Ruppel Stephen C. et al. 2010. Preliminary Classification of Matrix Pores in Mudrocks *Gulf Coast Association of Geological Societies Transactions* **60**: 435-441.

He, Man-Chao, Jian Zhao. 2013. Methane Adsorption on Graphite(0001) Films: A first-Principles Study. *Chinese Physics B* **22** (1). 016802.

Kang, S. M., E. Fathi, R. J. Ambrose et al. 2011. Carbon Dioxide Storage Capacity of Organic-Rich Shales. *Spe Journal* **16** (4): 842-855..

Kaxiras, Efthimios, K. C. Pandey. 1988. Energetics of Defects and Diffusion Mechanisms in Graphite. *Physical Review Letters* **61** (23): 2693-2696. http://link.aps.org/doi/10.1103/PhysRevLett.61.2693.

Kelemen, S. R. , M. Afeworki, M. L. Gorbaty et al. 2007. Direct Characterization of Kerogen by X-ray and Solid-State 13C Nuclear Magnetic Resonance Methods. *Energy Fuels* **21**: 1548-1561.

Kelemen, S. R., H. Freund, M. L. Gorbaty et al. 1999. Thermal Chemistry of Nitrogen in Kerogen and Low-Rank Coal. *Energy & Fuels* **13** (2): 529-538.

Kelemen, S. R., M. L. Gorbaty, P. J. Kwiatek. 1994. Quantification of Nitrogen Forms in Argonne Premium Coals. *Energy & Fuels* **8** (4): 896-906.

Knicker, H., A. W. Scaroni, P. G. Hatcher. 1996. C-13 and N-15 NMR Spectroscopic Investigation on the Formation of Fossil Algal Residues. *Organic Geochemistry* **24** (6-7): 661-669.

Lorant, F., F. Behar. 2002. Late Generation of Methane from Mature Kerogens. *Energy & Fuels* **16** (2): 412-427.

Gaussian 09, 2009. Wallingford CT, Gaussian, Inc.

Martin, M. G., J. I. Siepmann. 1998. Transferable Potentials for Phase Equilibria. 1. United-Atom Description of n-Alkanes. *Journal of Physical Chemistry B* **102** (14): 2569-2577.
Martin, Marcus G. 2013. MCCCS Towhee: a Tool for Monte Carlo Molecular Simulation. *Molecular Simulation* **39** (14-15): 1184-1194.

McCarthy, Kevin., Katherine. Rojas, Martin. Niermann et al. 2011. Basic Petroleum Geochemistry for Source Rock Evaluation. *Oilfield Review* **23**: 32-43.

McDonald, I. R. 2002. NpT-ensemble Monte Carlo Calculations for Binary Liquid Mixtures (Reprinted from Molecular Physics, vol 23, pg 41-58, 1972). *Molecular Physics* **100** (1): 95-105.

NIST. http://webbook.nist.gov/chemistry/fluid/.

Norman, G. E., V. S. Filinov. 1969. Investigations of Phase Transitions by a Monte-Carlo Method. *High Temperature* **7** (2): 216-&.

Patience, R. L., M. Baxby, K. D. Bartle et al. 1992. The Functionality of Organic Nitrogen in Some Recent Sediments from the Peru Upwelling Region. *Organic Geochemistry* **18** (2): 161-169.

Saxby, J. D., A. J. R. Bennett, J. F. Corcoran et al. 1986. Petroleum Generation - Simulation Over 6-years of Hydrocarbon Formation From Torbanite and Brown Coal in a Subsiding Basin. *Organic Geochemistry* **9** (2): 69-81.

Scott, A.R. Composition and Origin of Coalbed Gases from Selected Basins in the United States. *Birmingham, Alabama*, Vol. 1, 207-222.

Shao, Yuyan, Sheng Zhang, Mark H. Engelhard et al. 2010. Nitrogen-Doped Graphene and its Electrochemical Applications. *Journal of Materials Chemistry* **20** (35): 7491-7496. Shayeganfar, F., M. Neek-Amal. 2012. Methane Molecule Over the Defected and Rippled Graphene Sheet. *Solid State Communications* **152** (15): 1493-1496.

Steele., William. 1973. The physical interaction of gases with crystalline solids. *Surface Science* **36** (1): 317–352.

Suleimenova, A., K. D. Bake, A. Ozkan et al. 2014. Acid Demineralization with Critical Point Drying: A Method for Kerogen Isolation that Preserves Microstructure (in English). *Fuel* **135**: 492-497.

Swami, Vivek, Christopher R. Clarkson, Antonin Settari. Non-Darcy Flow in Shale Nanopores: Do We Have a Final Answer? Proc.

Tang, Y., P. D. Jenden, A. Nigrini et al. 1996. Modeling Early Methane Generation in Coal. *Energy & Fuels* **10** (3): 659-671.

Thierfelder, C., M. Witte, S. Blankenburg et al. 2011. Methane Adsorption on Graphene from First Principles Including Dispersion Interaction. *Surface Science* **605** (7-8): 746-749.

Tissot B.P. , Welte D.H. 1984. Kerogen: Composition and Classification. In *Petroleum Formation and Occurrence* Berlin ; New York Springer-Verlag.

Ungerer, P. , J. Collell, M. Yiannourakou. 2015a. Molecular Modeling of the Volumetric and Thermodynamic Properties of Kerogen: Influence of Organic Type and Maturity. *Energy Fuels* **29** (1): 91-105.

Ungerer, Philippe, Julien Collell, Marianna Yiannourakou. 2015b. Molecular Modeling of the Volumetric and Thermodynamic Properties of Kerogen: Influence of Organic Type and Maturity. *Energy & Fuels* **29** (1): 91-105.

Wang Yin, Feng Yamin, Meng Gaoxiang et al. 2015. Methane Adsorption on Intrinsic, Vacancy and N-doped Graphene: A First-Principles Study. *Physica Status Solidi*

APPENDIX

SOLUTIONS OF EQUATIONS

$$V_{LJ} = 4\varepsilon \left[\left(\frac{\sigma}{r}\right)^{12} - \left(\frac{\sigma}{r}\right)^{6} \right] \quad (1)$$

By extracting the first derivative of the Lenard-Jones potential, we can obtain the r_{min} in function of σ when $\frac{\partial V_{LJ}}{\partial r} = 0$ therefore:

$$\frac{\partial V_{LJ}}{\partial r} = 4\varepsilon(-12)\sigma^{12}r^{-13} - 4\varepsilon(-6)\sigma^{6}r^{-7} = 0$$

$$r_{min} = \sqrt[6]{2}\sigma$$

By evaluating r_{min} into V_{LJ} we can determine epsilon value:

$$V_{LJ} = 4\varepsilon \left[\left(\frac{\sigma}{\sqrt[6]{2}\sigma}\right)^{12} - \left(\frac{\sigma}{\sqrt[6]{2}\sigma}\right)^{6} \right]$$

$$V_{LJ} = 4\varepsilon \left[\left(\frac{1}{\sqrt[6]{2}}\right)^{12} - \left(\frac{1}{\sqrt[6]{2}}\right)^{6} \right]$$

$$V_{LJ} = -\varepsilon$$

V_{LJ} and σ are read from the Lenard Jones curve that is fitted using quantum mechanics calculations. Epsilon and Sigma values are needed for Monte Carlo Calculations.

Equation (2) is called the Steele Wall and places a 10-4 Lennard-Jones wall representing graphite in the simulation boxes in Grand Canonic Monte Carlo Calculations. The Steele Wall has the following form:

$$V(z) = \varepsilon_W \left[\frac{2}{5} \left(\frac{\sigma_{sf}}{z} \right)^{10} - \left(\frac{\sigma_{sf}}{z} \right)^4 - \frac{\sigma_{sf}}{[3\Delta(z+0.61\Delta)^3]}^4 \right] \quad (2)$$

where

$$\varepsilon_w = 2 \, \pi \, \varepsilon_{sf} \, \rho_s \, \sigma_{sf}^2 \, \Delta$$

All the parameters of the above equation are implemented in *Towhee* software (Martin 2013).

 please see reference for further information (Steele, 1973)

$$\rho_{calc-CH4} = \frac{\rho_{number} M_{CH4}}{N_A} \quad (3)$$

From Langmuir adsorption isotherm Figure 6, we have that $n_{ads} = 250 mol$. The volume size of the first is 77.3 Å $\times$77.3 Å$\times$ 3.8 Å with a volume of 2.27E-20 cm^3, where 3.8 Å is the Van der Waals radii of methane molecule. Therefore for the first layer of adsorbed gas, we have:

$$\rho_{calc-CH4} = \frac{(250/2.27E^{-20})16}{6.02252E^{+23}} = 0.3\frac{gr}{ml}$$

To calculate the number of excess molecules we have to subtract the bulk density of methane (NIST values) from the calculated density of methane that starts in the "second" layer of methane in a nanopore of 4nm (see Figure 3) times the Van der Waals radii of methane molecule:

$$n_{excess} = \frac{[\sum_{i=2}^{N}(\rho_{calc-CH4} - \rho_{bulk-CH4})V_{3.8}] * N_A}{M_{CH_4}} \quad (4)$$

So for N=2-9, at typical shale gas reservoir conditions $P_{res=}$4000 psia

$$n_{excess} = \frac{(0.2-0.154)*2.27E^{-20}*6.022E+23}{16} + 21.88 + 10.579 + 4.680 + 9.779 + 12.379 +$$

$$18.578 + 45.\ 976\ 128.068 = 290 \text{ mol}$$

To calculate the adsorbed-gas amount in moles, reading the Langmuir storage capacity in moles representing the maximum adsorbed amount of methane in the pore from Figure 13 for 1N that is the same for pristine organic nanopores $G_{SL} = 480\ mol$ at P=4000 psia and P_L=500, we have:

$$G_a = G_{SL} \frac{p}{p+p_L} \quad (5)$$

$$G_a = 480 \frac{4000}{4000+500} = 426 mol$$